View Article Online / Journal Homepage / Table of Contents for this issue
Dynamic Article Links

CrystEngComm

Cite this: *CrystEngComm*, 2012, **14**, 4713–4718

www.rsc.org/crystengcomm

PAPER

Role of point defects on the enhancement of room temperature ferromagnetism in ZnO nanorods

P. Sundara Venkatesh,[a] V. Purushothaman,[a] S. Esakki Muthu,[b] S. Arumugam,[b] V. Ramakrishnan,[c] K. Jeganathan*[a] and K. Ramamurthi[d]

Received 19th January 2012, Accepted 20th April 2012
DOI: 10.1039/c2ce25098e

Vertically aligned undoped ZnO nanorod arrays (NRAs) have been fabricated on silicon (111) substrates by radio frequency magnetron sputtering. The structural studies illustrate a hexagonal wurtzite structure of the ZnO NRAs with compressive stress. Raman analysis of the E_2^{high} phonon mode corroborates the partial relaxation of stress in NRAs by the post growth treatment under oxygen and vacuum atmospheres. The anomalous Raman modes have been attributed to the local vibrations and it corresponds to the silent modes of wurtzite ZnO. The appearance of forbidden modes illustrates the breakdown of the Raman selection rules. The role of point defects on the ferromagnetic behaviour of NRAs was analyzed by optical transitions and correlated with the magnetic properties. Post growth treatment of NRAs under oxygen and vacuum atmospheres significantly suppresses the point defects owing to the enhancement of the crystalline quality. The temperature dependent zero-field cooled and field cooled magnetizations reveal the coexistence of antiferromagnetism and ferromagnetism below 7 K. However, the ferromagnetism is dominant and stable between 7 K and room temperature. The decrease of ferromagnetism in NRAs is directly associated with the compensation of point defects such as zinc and oxygen vacancies as substantiated by the radiative transition between shallow donor and acceptor energy levels. These results confirm that point defects play an important role in enhancing the room temperature ferromagnetism in ZnO NRAs.

Published on 23 April 2012. Downloaded by Michigan State University on 16/01/2016 07:26:07.

1. Introduction

Zinc oxide (ZnO) is a unique semiconductor material with a wide direct band gap of 3.37 eV and a relatively large exciton binding energy of 60 meV at room temperature. In recent years, it has attracted increasing interests in the fields of optoelectronics and spintronics. The theoretical prediction of room temperature ferromagnetism (RTFM) in a diluted magnetic semiconductor (DMS) triggered considerable attention in the field of spintronics, which could pave the way for the use of spin in addition to charge in semiconductor devices.[1] Many research groups have continued to pay considerable attention and have proved experimentally that DMS can exhibit RTFM.[2] Although the origin of ferromagnetism in oxide DMS is still not clear, the segregation of magnetic clusters is believed to explain the ferromagnetic behavior of oxide semiconductors.[3]

The magnetic properties of the oxide semiconductors are not directly related to the existence of the transition metal (TM) ions but strongly depend on the defects in the semiconductors. Hence, the growth conditions and post growth treatments play an important role in ferromagnetic nature of the materials since they can create point defects in oxide semiconductors which are similar to carrier doping. Thus, the defects could introduce RTFM in non-magnetic semiconductors.[4]

The observation of ferromagnetism in TM doped ZnO at and above room temperature makes it a potential candidate in the field of spintronics. The origin of ferromagnetism in TM doped ZnO is due to the significance of the point defects as well as the secondary phases, which leads to the ferromagnetic ordering of the materials and increases the Curie temperature (T_c). On the other hand, the ferromagnetic behaviour of undoped ZnO solely depends on the point defects such as oxygen vacancies (V_o),[5] oxygen interstitials (O_i),[6] Zn vacancies (V_{Zn})[7] and Zn interstitials (Zn_i).[8]

In order to develop ZnO based nanoscale functional devices, the fabrication of high quality one dimensional (1D) nanostructures are essential. Recently, the vertical aligned nanowire arrays have received good attention due to their applications in semiconductor industries for device fabrication. The metal catalytic assisted approach is widely employed for the fabrication

[a]*Centre for Nanoscience and Nanotechnology, School of Physics, Bharathidasan University, Tiruchirappalli, 620 024, India. E-mail: kjeganathan@yahoo.com*
[b]*Centre for High Pressure Research, School of Physics, Bharathidasan University, Tiruchirappalli, 620 024, India.*
[c]*Department of Laser Studies, School of Physics, Madurai Kamaraj University, Madurai, 625 021, India.*
[d]*Crystal growth and Thin film Laboratory, School of Physics, Bharathidasan University, Tiruchirappalli, 620 024, India.*

View Article Online

Published on 23 April 2012. Downloaded by Michigan State University on 16/01/2016 07:26:07.

of self-assembled ZnO nanostructures. However, these metal catalysts like Au will incorporate into the growing lattice of the nanostructures and reduce the efficiency of the devices.[9,10] Consequently, it is necessary to develop catalyst-free growth techniques for ZnO nanostructures. Among the various deposition methods, sputtering deposition is one of the most favorable and facile physical vapor deposition techniques in terms of scale-up and mass production[11] with superior structural quality as compared to chemical and solution methods.[12] In this method, one can easily manipulate the growth of the nanostructures by varying the deposition parameters such as sputtering pressure, substrate temperature and substrate–target distance. It is one of the least investigated techniques in the fabrication of ZnO nanostructures.[13–16] Furthermore, 1D nanostructures explore the possibility of engineering defects due to large surface to volume ratios. In the present work, we report the growth of well aligned ZnO nanorod arrays (NRAs) on the silicon (111) substrates by radio frequency (RF) magnetron sputtering without metal catalysts. The structural, optical and magnetic properties of ZnO NRAs are described and the role of point defects on the origin of the ferromagnetism and their exchange interactions are discussed on the basis of the optical transitions.

2. Experimental section

The vertically aligned undoped ZnO NRAs have been fabricated under low pressure by plasma assisted RF magnetron sputtering technique at elevated temperature on Si (111) substrates. A 2-inch target of pure ZnO (99.999%) was prepared by a simple solid state reaction method. Prior to deposition, the target was pre-sputtered for 15 min to remove the surface impurities on the target. The chamber was evacuated to the base pressure of 5×10^{-6} mbar and the deposition was carried out under a pure Ar atmosphere at a pressure of 6×10^{-3} mbar. The target to substrate distance was kept constant at 50 mm and the deposition was performed for 1 h at 550 °C with RF power of 140 W. To understand the role of impurities which induce or annihilate the magnetic interactions in 1D nanostructures, the as-grown (AG) NRAs are subjected to an annealing process at 500 °C for 30 min under an oxygen (0.1 mbar) and vacuum (1×10^{-5} mbar) environment.

The phase purity and crystallographic orientation of the ZnO NRAs were characterized by X-ray diffraction (XRD) patterns using a Rigaku X-ray diffractometer with Cu-Kα radiation of wavelength λ = 1.5406 Å. The surface morphology of the samples was studied using a field emission scanning electron microscope (FESEM, Carl Zeiss, Σigma). Micro-Raman scattering measurements were carried out by a LabRam HR800 Raman spectrometer at an excitation wavelength of 632.8 nm with a spot size of ~ 1μm in the quasi-back scattering geometry. The point defects and crystalline nature of the ZnO NRAs were analyzed by photoluminescence (PL) measurement using a He-Cd laser with an excitation wavelength of 325 nm. The magnetic properties of the ZnO NRAs were studied by a physical property measurement system (PPMS – 9T) Vibrating Sample Magnetometer (VSM) module (Quantum Design, USA) in the temperature range between 2 and 300 K.

3. Results and discussion

Fig. 1(a) depicts the XRD spectra of as-grown (AG), vacuum annealed (VA) and oxygen annealed (OA) ZnO NRAs. All the peaks can be indexed, resulting in the wurtzite hexagonal structure of ZnO NRAs. The relatively dominant (002) reflection of the ZnO NRAs implies that most of the NRAs are aligned vertically along the *c*-axis.[17] The presence of a weak (103) reflection implies that a significantly feeble number of ZnO NRAs are aligned in this direction. This illustrates the quasi alignment of NRAs along the *c*-axis. In addition to this, a weak reflection at around 64.5° corresponds to SiO_2.[18] It provides evidence for the presence of an SiO_2 layer on the top surface of the silicon substrate, which may be formed due to the oxidation of the silicon during the early stage of growth and followed by a post growth process. The (002) peak position of the AG ZnO NRAs (34.39°) is less than the bulk value (34.45°), indicating that the NRAs are in a state of uniform compressive stress.[19] It is worth noting that the (002) peak position of the VA and OA NRAs shifts about 0.02° linearly towards its bulk value as shown in Fig. 1(b). This provides evidence for the relaxation of the compressive stress due to the post growth treatment. The compressive stress in the AG NRAs has its origin in the imperfection of the crystallites during growth.[20,21] The interplanar spacing (*d*) and 2*θ* variations of AG

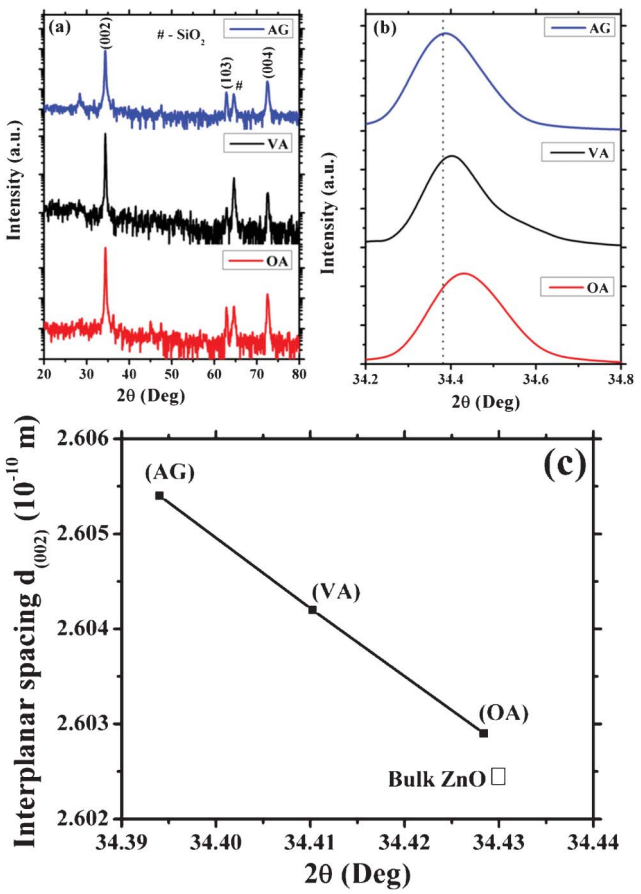

Fig. 1 (a) Typical X-ray diffraction pattern of vertically aligned undoped ZnO NRAs on silicon (111) substrate, (b) (002) peak position of AG, VA and OA undoped ZnO NRAs and (c) interplanar spacing (*d*) and 2*θ* variations of AG and post annealed (OA, VA) ZnO NRAs.

 This journal is © The Royal Society of Chemistry 2012

View Article Online

Published on 23 April 2012. Downloaded by Michigan State University on 16/01/2016 07:26:07.

and post annealed ZnO NRAs from its bulk value are shown in Fig. 1(c).

Fig. 2 (a) and (b) show the FESEM images of the ZnO NRAs grown on silicon (111) substrates. These images confirm that NRAs are well aligned normal to the substrate with smooth surfaces and nearly uniform diameter along the axial direction. The FESEM images also reveal the hexagonal cross section along the *c*-axis. The length of the ZnO NRAs is around 1.5 μm and the average diameter is about 350 nm.

Micro-Raman scattering is one of the most powerful tools to analyze the structural, optical and electrical properties of the nanomaterials. Fig. 3 shows the room temperature micro-Raman spectra of the undoped ZnO NRAs, grown under identical conditions and subordinated to various post growth treatments. In the back-scattering geometry, the spectra are recorded with the incident laser light exactly perpendicular to the top surface of the aligned ZnO NRAs, *i.e.*, the incident laser light is parallel to the *c*-axis of the NRAs. In this configuration, E_2 and A_1(LO) are the only allowed modes of vibrations for ZnO, whereas the other modes are forbidden according to the Raman selection rules.[22]

A sharp peak at 99.7 cm^{-1} corresponds to the E_2^{low} phonon mode of ZnO, which is attributed to the lattice vibrations of zinc

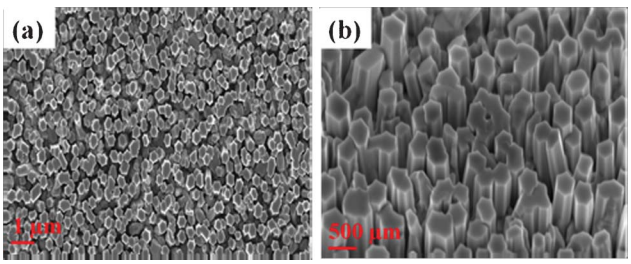

Fig. 2 FESEM images of AG undoped ZnO NRAs. (a) Top view and (b) 60° tilted view.

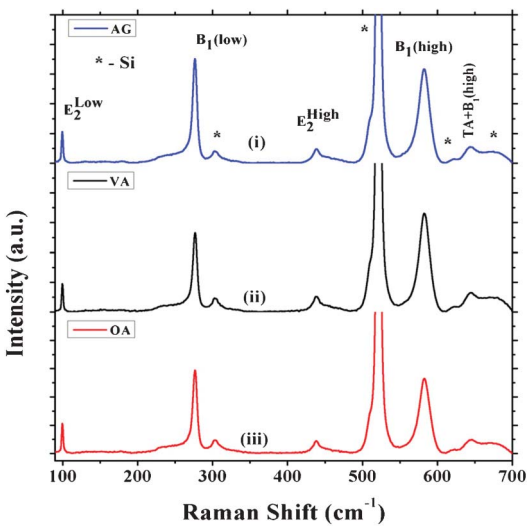

Fig. 3 Room temperature Raman spectra of vertically aligned AG and post annealed undoped ZnO NRAs recorded in the back-scattering geometry. (i) As-grown (AG), (ii) vacuum annealed (VA) and (iii) oxygen annealed (OA).

atoms. E_2^{high} phonon mode is typically used to describe the strain, crystalline nature and phase orientation. It is well known that the E_2^{high} phonon mode at 437 cm^{-1} is used to characterize the stress in the ZnO lattice; these vibrations are related to the lattice vibration of the oxygen atoms and indicate the wurtzite phase of ZnO.[23] The Lorentz fitted E_2^{high} mode at 438.9 cm^{-1} of the AG ZnO NRAs was blue shifted about 1.9 cm^{-1} as compared to the standard value. The shift in E_2^{high} phonon mode describes that the AG ZnO NRAs are under compressive strain.[24] The E_2^{high} peak of VA and OA ZnO NRAs was observed at 438.6 cm^{-1} and 438.3 cm^{-1} respectively. The E_2^{high} peak of the annealed NRAs was red shifted as compared to the AG NRAs which demonstrates that the compressive strain in ZnO NRAs was partially relaxed due to the post growth treatment under vacuum and oxygen atmospheres. The compressive stress was estimated by using $\Delta\omega = 4.4\sigma$ (GPa)[24] (σ is the stress and $\Delta\omega$ is the peak shift of the E_2^{high} phonon mode) and shown in Table 1.

Thus, the compressive stress of the AG ZnO NRAs is 0.432 GPa and the stress value of the annealed samples decreases as compared to AG NRAs. It depicts that the post growth treatment enhances the crystalline nature and partially relaxes the stress in the AG NRAs. The estimated compressive stress is smaller than the ZnO films grown on the silicon substrate,[25] which is due to the relaxation effect in the nanorods. Raman modes at around 302, 520, 610 and 670 cm^{-1} correspond to the optic and acoustic modes of the silicon substrate, attributed to 2TA (X), LO, a combination of TA + TO phonons in the Σ direction due to the second order processes and a two phonon mode respectively.[26]

The peak at 582 cm^{-1} can be attributed to either the E_1(LO) or B_1(high) modes. However, it is reported that the E_1(LO) mode observed at 581 cm^{-1} arises due to the oxygen deficiency such as oxygen vacancies.[27] In our case, the oxygen vacancies are present only in AG ZnO NRAs and it is compensated by the post growth treatments as explained in PL measurements. The position and intensity of the peak at 582 cm^{-1} remain the same for the all samples. Hence, it could not be assigned to E_1(LO). Due to the small dispersion along the Brillouin zone, the observed peaks at 276 and 582 cm^{-1} can be attributed to silent modes [B_1(low) & B_1(high)] of ZnO.[28] Furthermore, the B_1(low) mode is located near to the region of low two phonon density of states (DOS) while the B_1(high) mode is near to the region of high two phonon DOS. Hence, we observed that both B_1(low) and B_1(high) modes exhibit comparable intensities and the width of the B_1(low) mode is one third of the width of B_1(high) which agrees well with the earlier report.[29] Thus, the appearance of these morphic modes further confirms that ZnO NRAs are quasi *c*-axis oriented.

Fig. 4(a) shows the room temperature PL spectra of the ZnO NRAs grown under identical conditions, but subjected to different post growth treatments under oxygen and vacuum

Table 1 Stress and FWHM of the AG and post-annealed undoped ZnO NRAs

Sample	E_2^{high} (cm^{-1})	FWHM (cm^{-1})	Stress (GPa)
AG	438.9	13.06	0.432
VA	438.6	12.69	0.364
OA	438.3	12.42	0.295

View Article Online

Published on 23 April 2012. Downloaded by Michigan State University on 16/01/2016 07:26:07.

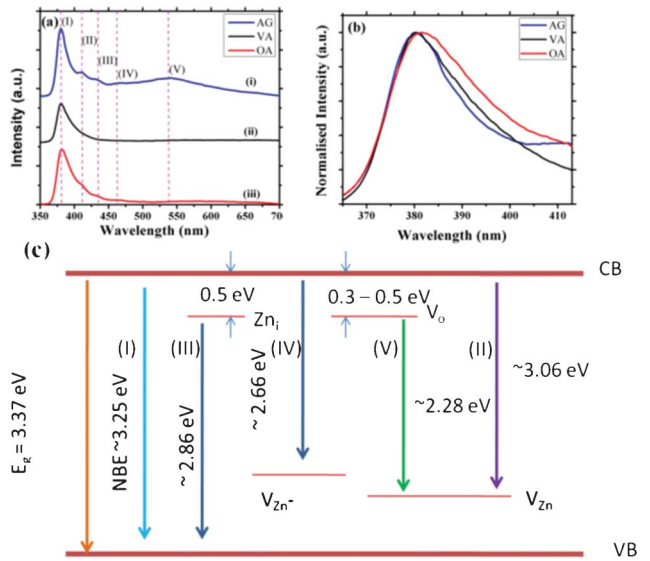

Fig. 4 (a) Room temperature photoluminescence spectra of AG and post annealed undoped ZnO NRAs. (i) As-grown (AG), (ii) vacuum annealed (VA) and (iii) oxygen annealed (OA). (b) Enlarged view of the near band edge (NBE) emission of the PL spectra. (c) Energy band diagram of ZnO NRAs ascribed from PL transitions.

atmospheres. The UV emission around 380 nm is well understood as a near band edge (NBE) emission[30] and various defects such as vacancies and interstitial sites are the culprits for the visible emission.[31] A linear relationship can be established with the intrinsic point defects in undoped ZnO including vacancies by optical transitions.

The PL spectrum of AG ZnO NRAs shows the UV (380 nm), violet (410 nm), blue (430 and 465 nm) and green (541 nm) emissions. The visible region of the PL spectra clearly illustrates the existence of point defects both in AG and OA ZnO NRAs. However, the green luminescence is absolutely suppressed in OA NRAs at 500 °C due to the passivation of oxygen vacancy induced point defects. Nevertheless, the violet and blue transitions can be related to the point defects of zinc such as zinc vacancies and interstitial zinc.[32] On the other hand, all the visible emissions are completely suppressed in the VA NRAs due to the recrystallization process. The surface adsorbed oxygen atoms are expected to diffuse into the oxygen vacancy site during the post growth process. The surface adsorbed oxygen atoms do not leave the surface as O_2 molecules and it is energetically less stable than the ZnO lattice. Hence, the oxygen vacancies are likely to be compensated by the interaction induced diffusion of surface atoms. The UV emission peak of VA and OA ZnO NRAs is slightly red shifted as compared to the AG ZnO NRAs. This shows the presence of small residual compressive stress in the AG NRAs and the strain was partially relaxed during the post growth treatments at high temperature, as evidenced by the red shift in the band gap of the ZnO NRAs[33] and it is clearly shown in the Fig. 4(b). These results corroborate with the XRD and Raman data and confirm the existence of compressive stress.

The zinc vacancy (V_{Zn}) will act as an acceptor and create an acceptor level above the valence band. It was accounted that the energy difference between the conduction band minimum and the zinc vacancy level (V_{Zn}) is about 3.06 eV.[34] This shows that the acceptor level is well above the valence band at about 0.3 eV. We believe that the observed peak at 410 nm is the electron transition from the conduction band to the V_{Zn} level and this transition provides clear evidence for the presence of zinc vacancies in the ZnO NRAs. Interstitial zinc (Zn_i) produces the shallow and deep level donors at 0.5 and 1.3 eV below the bottom of the conduction band. In the emission spectra, the peak at 430 nm is assigned to the recombination of an electron from the shallow level donor of Zn_i to a hole in the valence band.[35] The blue emission at 465 nm corresponds to the transition electron from the conduction band to the singly ionized zinc vacancy (V_{Zn}^-), which lies around 2.66 eV below the conduction band.[32] A broad peak around 541 nm corresponds to oxygen vacancies and this green luminescence is attributed to the electron transition from the shallow donor level (V_o) to a shallow acceptor level (V_{Zn}).[36,37] These transitions confirm the existence of the oxygen and zinc vacancies in the AG ZnO NRAs. In the OA NRAs, the intensity of green luminescence is substantially suppressed which means that the oxygen vacancies are totally counterbalanced and the intensity of the blue luminescence is reduced considerably by the partial compensation of zinc vacancies. Hence, the only possible emission for the blue luminescence is the transition between conduction band and acceptor level. In the VA NRAs, the intensities of blue and green luminescence are totally suppressed by the consequence of the compensation of zinc and oxygen vacancies. Hence the defect mediated emissions are absent and only NBE emission is present in the VA NRAs. The emission spectra of the ZnO NRAs can be clearly explained using the energy level diagram as described in Fig. 4(c).

Fig. 5 shows the temperature dependent magnetization curves of AG and post annealed ZnO NRAs recorded at a constant field strength of 1000 Oe. The temperature dependent magnetization is recorded by performing zero field cooled (ZFC) and field cooled (FC) magnetization measurements at a temperature range of 2 K–300 K. In the entire temperature range, ZFC and FC curves do not show any transition from the ferromagnetic to the paramagnetic phase, which reveals that the Curie temperature of the undoped ZnO NRAs is well above the room temperature (300 K). At a low temperature, around 7 K, there is a clear cusp in both ZFC and FC temperature dependent

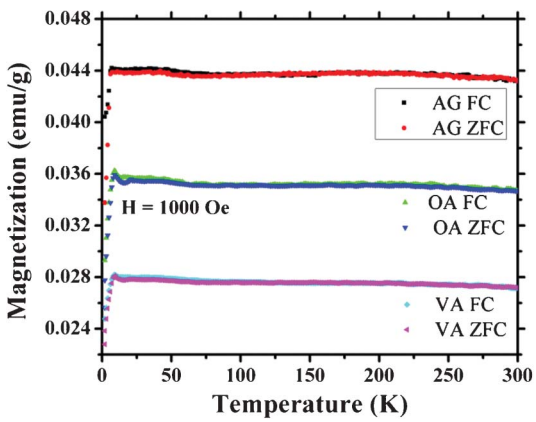

Fig. 5 Temperature dependent ZFC and FC magnetization curves recorded under constant field of 1 kOe for ZnO NRAs.

 This journal is © The Royal Society of Chemistry 2012

View Article Online

Published on 23 April 2012. Downloaded by Michigan State University on 16/01/2016 07:26:07.

magnetization curves, which indicates a spin-glass behavior.[38–41] This spin-glass behavior correlates the coexistence of ferromagnetic and antiferromagnetic interaction. However, the ferromagnetic phase is still strongly dominant and stable over the whole range of temperatures (2–300 K). At low temperatures (2 K), the value of coercivity is large as compared to room temperature and it provides a strong evidence for the existence of ferromagnetism along with a small antiferromagnetic nature of ZnO NRAs.

The magnetization *versus* magnetic field (M–H) curves of AG and post annealed (both oxygen and vacuum at 500 °C) ZnO NRAs is shown in Fig. 6. The hysteresis loops along ZFC and FC clearly indicate that NRAs have indisputable RTFM. The actual magnetization of AG and post annealed ZRAs is determined by subtracting the diamagnetic contribution of the silicon substrate from the raw data. The unit of magnetization is converted into emu g^{-1} by considering the diameter, length and density with hexagonal geometry of the nanorods.

ZFC and FC curves of AG NRAs show very high stable FM which can be related to the presence of oxygen and zinc vacancies as revealed by PL transitions in visible region. On the other hand, the magnetization is considerably decreased due to the compensation of oxygen vacancies as the NRAs were annealed under an oxygen atmosphere. However zinc vacancies are present as evidenced by the blue luminescence at 410 nm. The complete suppression of point defects in VA NRAs gives rise to the softening of RTFM but is unable to eliminate the FM, as opposed to the absence of blue and green emissions. The presence of RTFM in VA samples where no vacancies of oxygen and zinc are observed by PL transitions indicate that vacancy induced point defects alone are not solely responsible for the magnetic moment in undoped ZnO NRAs. Thus, one can conclude that the intrinsic defects and surface related impurity transitions are expected greatly to be responsible for the origin of FM in 1D ZnO NRAs. As expected, the defect induced ferromagnetism (FM) would be decreased by the improvement of the crystalline nature through the annealing processes. The magnetization decreases considerably after annealing both in oxygen and vacuum at 500 °C for 30 min. The saturation magnetization and coercivity of ZnO NRAs are shown in Table 2. The coercivity is enhanced at lower temperatures (*i.e.*, 2 K) as compared to room temperature (*i.e.*, 300 K) in the ZnO NRAs. This is called a broadening effect which is a classical behaviour of the magnetic materials at low temperature. The origin of the RTFM in pure ZnO NRAs may be attributed to the exchange interactions between unpaired electron spins arising from either vacancies[42] or surface defects.

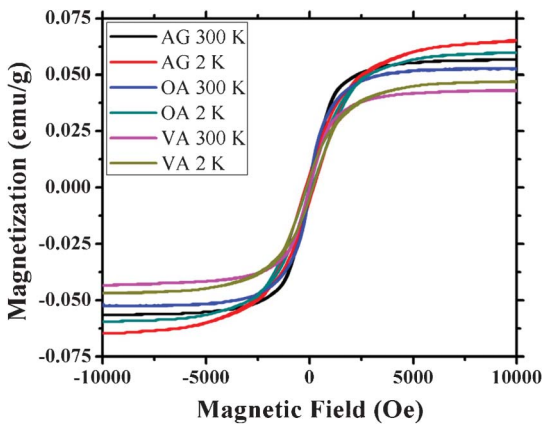

Fig. 6 Magnetic hysteresis loops of the undoped ZnO NRAs (as-grown and post-annealed (OA and VA)) at 2 and 300 K.

4. Conclusion

In summary, vertically aligned ZnO NRAs have been grown on the silicon substrates by RF magnetron sputtering technique in pure argon atmosphere. XRD patterns of the ZnO NRAs indicate the existence of the residual compressive stress along the *c*-axis which is partially relaxed by the post growth treatments. Further, micro-Raman spectra provide conclusive evidence for the partial relaxation of the compressive stress in NRAs from the peak position of the non-polar phonon mode E_2(high). The intra-band optical transitions provide a strong evidence for the existence of vacancy mediated point defects which is found to be responsible for the enhancement of RTFM in undoped ZnO NRAs as corroborated by a clear hysteresis loop from the M–H curve. The ferromagnetism decreases with post growth treatment of ZnO NRAs in both oxygen and vacuum atmospheres owing to the compensation of point defects and it provides a strong confirmation that the enhancement of RTFM is expected to be due to vacancy mediated exchange interactions between the unpaired electron spins in undoped ZnO NRAs.

Acknowledgements

KJ acknowledges financial support from the Department of Science and Technology (DST) - Nanomission, Govt. of India under the contract no. SR/NM/NS-77/2008 for infrastructural facilities. KJ and KR thank the DST for the financial support under the scheme of Fund for Improvement of Science and Technology Infrastructure in Universities and Higher Educational Institutes (FIST). One of the authors (PSV) acknowledges the award of a UGC – meritorious fellowship, UGC, Govt. of India. SA would like to acknowledge the DST, UGC and CSIR for their partial financial support. The authors would like to thank Miss P. Sangeetha for experimental assistance with Raman spectroscopy.

Table 2 Magnetization and coercivity of the AG and post-annealed undoped ZnO NRAs

	As-grown		Oxygen annealed		Vacuum annealed	
Parameters	2 K	300 K	2 K	300 K	2 K	300 K
Saturation magnetization (emu g^{-1})	0.065	0.056	0.059	0.052	0.047	0.042
Coercivity (Oe)	~ 198	~ 14	~ 158	~ 11	~ 130	~ 10

View Article Online

Published on 23 April 2012. Downloaded by Michigan State University on 16/01/2016 07:26:07.

References

1 T. Dietl, H. Ohno, F. Matsukura, J. Cibert and D. Ferrand, *Science*, 2000, **287**, 1019.
2 Y. J. Kim, S. Thevuthasan, T. Droubay, A. S. Lea, C. M. Wang, V. Shutthanandan, S. A. Chambers, R. P. Sears, B. Taylor and B. Sinkovic, *Appl. Phys. Lett.*, 2004, **84**, 3531.
3 N. H. Hong, V. Brizé and J. Sakai, *Appl. Phys. Lett.*, 2005, **86**, 082505.
4 K. R. Kittilstvet, N. S. Norberg and D. R. Gamelin, *Phys. Rev. Lett.*, 2005, **94**, 147209.
5 B. Huang, D. Zhu and X. Ma, *Appl. Surf. Sci.*, 2007, **253**, 6892.
6 G. Brauer, W. Anwand, W. Skorupa, J. Kuriplach, O. Melikhova, C. Moisson, H. von Wenckstern, H. Schmidt, M. Lorenz and M. Grundmann, *Phys. Rev. B: Condens. Matter Mater. Phys.*, 2006, **74**, 045208.
7 W. Yan, Z. Sun, Q. Liu, Z. Li, Z. Pan, J. Wang, S. Wei, D. Wang, Y. Zhou and X. Zhang, *Appl. Phys. Lett.*, 2007, **91**, 062113.
8 T. Shi, Z. Xiao, Z. Yin, X. Li, Y. Wang, H. He, J. Wang, W. Yan and S. Wei, *Appl. Phys. Lett.*, 2010, **96**, 211905.
9 E. R. Hemesath, D. K. Schreiber, E. B. Gulsoy, C. F. Kisielowski, A. K. Petford-Long, P. W. Voorhees and L. J. Lauhon, *Nano Lett.*, 2012, **12**, 167.
10 J. E. Allen, E. R. Hemesath, D. E. Perea, J. L. Lensch-Falk, Z.Y. Li, F. Yin, M. H. Gass, P. Wang, A. L. Bleloch, R. E. Palmer and L. J. Lauhon, *Nat. Nanotechnol.*, 2008, **3**, 168.
11 J. H. Park, H. K. Park, J. Jeong, W. Kim, B. K. Min and Y. R. Do, *J. Electrochem. Soc.*, 2011, **158**, K131–K135.
12 A. Janotti and C. G. Van de Walle, *Rep. Prog. Phys.*, 2009, **72**, 126501.
13 Z. F. Wu, X. M. Wu, L. J. Zhuge, X. M. Chen and X. F. Wang, *Appl. Phys. Lett.*, 2008, **93**, 023103.
14 S. W. Kang, S. K. Mohanta, Y. Y. Kim and H. K. Cho, *Cryst. Growth Des.*, 2008, **8**, 1458.
15 Z. F. Wu, X. M. Wu, L. J. Zhuge, B. Hong, X. M. Yang, X. M. Chen and Q. Chen, *Mater. Lett.*, 2010, **64**, 472.
16 Y. Y. Kim, B. H. Kong and H. K. Cho, *J. Cryst. Growth*, 2011, **330**, 17.
17 H.-J. Kim, K. Sung, K.-S. An, Y. K. Lee, C. G. Kim, Y.-H. Lee and Y. Kim, *J. Mater. Chem.*, 2004, **14**, 3396.
18 ICDD - JCPDS Card No. 89-3607.
19 X. J. Liu, C. Song, F. Zeng, X. B. Wang and F. Pan, *J. Phys. D: Appl. Phys.*, 2007, **40**, 1608.
20 W. Water and S.-Y. Chu, *Mater. Lett.*, 2002, **55**, 67.
21 Y.-C. Lee, S.-Y. Hu, W. Water, Y.-S. Huang, M.-D. Yang, J.-L. Shen, K.-K. Tiong and C.-C. Huang, *Solid State Commun.*, 2007, **143**, 250.
22 F. Wang, H. He, Z. Ye, L. Zhu, H. Tang and Y. Zhang, *J. Phys. D: Appl. Phys.*, 2005, **38**, 2919.
23 J. Serrano, F. J. Manjón, A. H. Romero, F. Widulle, R. Lauck and M. Cardona, *Phys. Rev. Lett.*, 2003, **90**, 055510.
24 F. Decremps, J. P. Porres, A. M. Saitta, J.C. Chervin and A. Polian, *Phys. Rev. B*, 2002, **65**, 092101.
25 S. Whangbo, H. Jang, S. Kim, M. Cho, K. Jeong and C. Whang, *J. Korean Phys. Soc.*, 2000, **37**, 456.
26 F. Singh, R. G. Singh, V. Kumar, S. A. Khan and J. C. Pivin, *J. Appl. Phys.*, 2011, **110**, 083520.
27 J. J. Wu and S. C. Liu, *J. Phys. Chem. B*, 2002, **106**, 9546.
28 J. Serrano, A. H. Romero, F. J. Manjón, R. Lauck, M. Cardona and A. Rubio, *Phys. Rev. B*, 2004, **69**, 094306.
29 F. J. Manjón, B. Marí, J. Serrano and A. H. Romero, *J. Appl. Phys.*, 2005, **97**, 053516.
30 D. C. Reynolds, D. C. Look, B. Jogai, C. W. Litton, T. C. Collins, W. Harsch and G. Cantwell, *Phys. Rev. B*, 1998, **57**, 12151.
31 Ü. Özgür, Ya. I. Alivov, C. Liu, A. Teke, M. A. Reshchikov, S. Doğan, V. Avrutin, S.-J. Cho and H. A. Morkoç, *J. Appl. Phys.*, 2005, **98**, 041301.
32 S. Bayan and D. Mohanta, *J. Appl. Phys.*, 2011, **110**, 054316.
33 X. Q. Meng, D. Z. Shen, J. Y. Zhang, D. X. Zhao, Y. M. Lu, L. Dong, Z. Z. Zhang, Y. C. Liu and X. W. Fan, *Solid State Commun.*, 2005, **135**, 179.
34 Z. Fang, Y. Wang, D. Xu, Y. Tan and X. Liu, *Opt. Mater.*, 2004, **26**, 239.
35 L.-L. Zhang, C.-X. Guo, J.-G. Chen and J.-T. Hu, *Chin. Phys.*, 2005, **14**, 586.
36 E. Gür, S. Tüzemen, K. Meral and Y. Onganer, *Appl. Phys. A: Mater. Sci. Process.*, 2009, **94**, 549.
37 C.-L. Hsu, S.-J. Chang, Y.-R. Lin, S.-Y. Tsai and I. C. Chen, *Chem. Commun.*, **2005**, 3571.
38 T. S. Herng, S. P. Lau, C. S. Wei, L. Wang, B. C. Zhao, M Tanemura and Y. Akaike, *Appl. Phys. Lett.*, 2009, **95**, 133103.
39 J. H. Park, M. G. Kim, H. M. Jang, S. Ryu and Y. M. Kim, *Appl. Phys. Lett.*, 2004, **84**, 1338.
40 S.-J. Han, T.-H. Jang, Y. B. Kim, B.-G. Park, J.-H. Park and Y. H. Jeong, *Appl. Phys. Lett.*, 2003, **83**, 920.
41 N. H. Hong, J. Sakai and A. Hassini, *J. Appl. Phys.*, 2005, **97**, 10D312.
42 S. Banerjee, M. Mandal, N. Gayathri and M. Sardar, *Appl. Phys. Lett.*, 2007, **91**, 182501.

 This journal is © The Royal Society of Chemistry 2012